

1 **Changes in global vegetation distribution and carbon fluxes in response to global**
2 **warming: simulated results from IAP-DGVM in CAS-ESM2**

3 Xiaofei Gao^{1,2}, Jiawen Zhu^{1*}, Xiaodong Zeng^{1,3}, Minghua Zhang⁴, Yongjiu Dai⁵,
4 Duoying Ji⁶, He Zhang¹

5 ¹*International Center for Climate and Environment Sciences, Institute of Atmospheric*
6 *Physics, Chinese Academy of Sciences, Beijing 100029, China*

7 ²*University of Chinese Academy of Sciences, Beijing 100049, China*

8 ³*Collaborative Innovation Center on Forecast and Evaluation of Meteorological*
9 *Disasters, Nanjing University of Information Science and Technology, Nanjing*
10 *210044, China*

11 ⁴*School of Marine and Atmospheric Sciences, Stony Brook University, NY 11790,*
12 *USA*

13 ⁵*School of Atmospheric Sciences, Sun Yat-Sen University, Guangzhou 510275, China*

14 ⁶*College of Global Change and Earth System Science, Beijing Normal University,*
15 *Beijing 100875, China*

16
17
18
19
20
21
22
23
24
25
26
27

*Corresponding author: Jiawen Zhu
28 Email: zhujw@mail.iap.ac.cn

ABSTRACT

29

30 Terrestrial ecosystems are an important part of Earth systems, and they are
31 undergoing remarkable changes in response to global warming. This study
32 investigates the response of terrestrial vegetation distribution and carbon fluxes to
33 global warming by using the new dynamic global vegetation model in the second
34 version of the Chinese Academy of Sciences (CAS) Earth System Model (CAS-
35 ESM2). We conducted two sets of simulations, the present-day simulation and the
36 future simulation, which were forced by the present-day climate during 1981–2000
37 and the future climate during 2081–2100, respectively, derived from RCP8.5 outputs
38 in CMIP5. CO₂ concentration is kept constant in all simulations to isolate CO₂-
39 fertilization effects. The results show an overall increase in vegetation coverage in
40 response to global warming, which is the net result of the greening in the mid-high
41 latitudes and the browning in the tropics. The results also show an enhancement in
42 carbon fluxes in response to global warming, including gross primary productivity,
43 net primary productivity and autotrophic respiration. We found that the changes in
44 vegetation coverage were significantly correlated with changes in surface air
45 temperature, reflecting the dominant role of temperature, while the changes in carbon
46 fluxes were caused by the combined effects of leaf area index, temperature, and
47 precipitation. This study applies CAS-ESM2 to investigate the response of terrestrial
48 ecosystems to climate warming. Even though the results are limited by isolating CO₂-
49 fertilization effects, this application is still favorable to better understand vegetation
50 processes and to further improve model parameterizations.

51 **Key words:** global warming, vegetation distribution, carbon flux, leaf area index,
52 surface air temperature

53 **Article Highlights:**

54 ● The projected vegetation coverage and carbon fluxes show an overall increase
55 under global warming.

56 ● Surface air temperature is the dominant driver of changes in vegetation
57 distribution.

58 ● Changes in carbon fluxes are caused by the combined effects of leaf area index,
59 temperature, and precipitation.

60 <https://doi.org/10.1007/s00376-021-1138-3>

61 **1. Introduction**

62 Terrestrial ecosystems are an important part of Earth systems. They regulate the
63 exchanges of energy and water mass between the land surface and atmosphere via
64 evapotranspiration and provide organic carbon via photosynthesis. The change in
65 terrestrial ecosystems is tightly coupled with climate, which is undergoing significant
66 warming (Diffenbaugh and Field, 2013; Zhu et al., 2016; Yin et al., 2018; Liu et al.,
67 2019). How terrestrial ecosystems respond to global warming has been a hot research
68 topic as the responses are of great significance for accurately projecting future
69 vegetation dynamics and climate change (Woodward, 1987; Nemani et al., 2003;
70 Schaphoff et al., 2016; Eric et al., 2018; Fan et al., 2019).

71 In response to global warming, land vegetation distribution and productivity have
72 shown considerable changes over the past few decades (Cramer et al., 2001; Fraser et
73 al., 2011; Cao et al., 2019). One of the significant changes is a poleward “greening”
74 expansion in the middle and high latitudes (Sturm et al., 2001; Walker et al., 2006; Bi
75 et al., 2013; Mao et al., 2016; Zhu et al., 2016; Piao et al., 2020; Tømmervik et al.,
76 2020). For example, forests in Europe were projected to expand northward and
77 contribute to a shrinkage of the tundra area (Shiyatov et al., 2005; Frost and Epstein,
78 2014; Kreplin et al., 2021), with a similar expansion found in North America (Field et
79 al., 2007, Yu et al., 2014). In Northeast China, Hu et al. (2021) found obvious
80 vegetation greening. The results shown by Madani et al. (2020) indicated increasing
81 trends in annual gross primary productivity (GPP) in the northern tundra and boreal
82 ecosystems. The greening of Arctic ecosystems has shown an increased biomass and
83 abundance in boreal shrubs (Myers-Smith et al., 2011, 2020; Mekonnen et al., 2021).
84 Several studies have reported that warming is a key factor that accelerates the
85 “greening” by enhancing vegetation photosynthesis and extending the length of the
86 growing season (Piao et al., 2007; Andreu-Hayles et al., 2011; Keenan and Riley,
87 2018). In the tropics, the response of vegetation to warming is different from that in
88 mid-high latitudes (Corlett, 2011). A number of studies have shown a decrease in the
89 tropical forest growth rate and productivity in response to warming, which could be
90 the consequence of a reduction in leaf photosynthesis under higher temperature (Clark
91 et al., 2003; Doughty and Goulden, 2008; Gao et al., 2019; Huang et al., 2019). The
92 decrease in water availability associated with higher temperature is reported to result

93 in a decrease in leaf area index (LAI) and net primary productivity (NPP) in Amazon
94 and South Africa and a decrease in forest coverage in the central and southern Mexico
95 (Mackay, 2007; Yu et al., 2014; Gang et al., 2017). These studies all indicate that
96 terrestrial ecosystems have undergone remarkable changes in vegetation distribution
97 and productivity due to global warming, and these changes will continue if global
98 warming continues in the future.

99 Nowadays, Dynamic Global Vegetation Models (DGVMs) have become widely
100 used tools to investigate and predict the responses of terrestrial ecosystems to future
101 climate change. They can simulate and project the patterns, dynamics and structure,
102 and biogeochemical cycles of vegetation under past, present and future climatic
103 conditions (Scheiter et al., 2013; Smith et al., 2014). Many DGVMs have been used to
104 run offline simulations with different climatic scenarios to predict the responses of
105 vegetation to changes in climate or atmospheric CO₂ (Woodward and Lomas, 2004;
106 Shafer et al., 2015; Zhang et al., 2015). In addition, some DGVMs are coupled with
107 general circulation models (GCMs) to investigate interactions between vegetation
108 dynamics and climate change (Raddatz et al., 2007; Brovkin et al., 2009; Quillet et al.,
109 2010; Hawkins et al., 2019; Wu et al., 2019; Arora et al., 2020; Shevliakova et al.,
110 2020; Yu et al., 2021).

111 However, the simulated vegetation responses to climate change by DGVMs
112 remain uncertain (Prentice et al., 2007; Sitch et al., 2008; Liu et al., 2018; Sulman et
113 al., 2019; Scheiter et al., 2020; Horvath et al., 2021). Falloon et al. (2012) reported
114 that DGVMs simulated different, even opposite vegetation changes in northern high

115 latitudes in response to climate change. In the North China Plain, the predicted
116 potential vegetation is bare ground, whereas in fact, it is dominated by irrigated
117 cropland (Suchul and Eltahir, 2018). South Asian savanna ecosystems are often
118 misinterpreted by DGVMs as degraded forests (Kumar and Scheiter, 2019). In
119 addition, the estimation of GPP often differed among DGVMs (McGuire et al., 2001;
120 Jung et al., 2007; Piao et al., 2013; Anav et al., 2015) due to different representations
121 of ecological processes and parameter uncertainties (Knorr and Heimann, 2001;
122 Gurney et al., 2004; De Kauwe et al., 2014). Gang et al. (2017) argued that large
123 uncertainties among DGVMs may relate to the differences in recognition of the
124 vegetation types and the land surface processes that evolved. These reported
125 uncertainties reflect the complexity of vegetation responses to climate change, and
126 thus more investigation is needed to understand vegetation processes and
127 parameterizations in DGVMs.

128 A new DGVM developed at the Institute of Atmospheric Physics (IAP-DGVM;
129 Zeng et al., 2014) has been coupled with the second version of the Chinese Academy
130 of Sciences Earth System Model (CAS-ESM2). The coupled results showed a good
131 performance in reproducing the present-day vegetation distribution and carbon fluxes
132 (Zhu et al., 2018). In addition, IAP-DGVM simulated a positive trend in LAI over
133 northern mid-high latitudes during the period 1972–2004, which was consistent with
134 that of LAI3g, with a significant correlation coefficient 0.48 ($P < 0.05$) (Fig. S1). The
135 consistency illustrates that IAP-DGVM has a good ability to reproduce the greening
136 trend of vegetation over northern mid-high latitudes in response to climate change

137 during the historical period. Thus, this study focuses on IAP-DGVM projections of
138 vegetation distribution and carbon fluxes in response to global warming in the future.
139 To narrow down the uncertainties in the forcing datasets, a method (seen Section 2) is
140 used to produce the forcing datasets based on multi-model outputs from the Coupled
141 Model Intercomparison Project Phase 5 (CMIP5) instead of using them directly. We,
142 on the one hand, report the simulated changes in vegetation distribution and carbon
143 fluxes in response to global warming. More importantly, we further investigate the
144 dominant driver of the changes and discuss the underlying causes. The investigation is
145 favorable for a better understanding of vegetation processes and for a further
146 improvement in the model parameterizations. Moreover, the results provide a valuable
147 sample for comparison not only for the CAS-ESM2 community but also for other
148 model communities.

149 **2. Model description and experimental design**

150 ***2.1. Model description***

151 IAP-DGVM, which was first released in 2014 (Zeng et al., 2014), was used in
152 this study. IAP-DGVM classifies natural plants into 14 plant functional types (PFTs)
153 and does not simulate crops now (Table S1). The vegetation model has made
154 significant developments that mainly include the shrub sub-model (Zeng et al., 2008;
155 Zeng, 2010), the process-based fire parameterization of intermediate complexity (Li et
156 al., 2012) and the new establishment and competition parameterization schemes
157 (Song, 2016). These characteristics improve the performance of IAP-DGVM in

158 simulating the fractional coverage of present-day vegetation and land carbon fluxes
159 (Zeng, 2010; Zeng et al., 2014; Zhu et al., 2018). Thus, IAP-DGVM has been coupled
160 with CAS-ESM2 to investigate vegetation-climate interactions (Zhu et al., 2018;
161 Zhang et al., 2020).

162 **2.2. Experimental design**

163 This study aims to investigate the possible changes in vegetation distribution and
164 carbon fluxes under global warming. The scenario for Representative Concentration
165 Pathway 8.5 (RCP8.5) was selected to represent a possible scenario of future global
166 warming and the climate in the period 2081–2100 was selected to represent the future
167 climate. We downloaded atmospheric forcing variables, six-hourly precipitation and
168 solar radiation, three-hourly surface air temperature, surface pressure, specific
169 humidity and wind, from outputs of historical and RCP8.5 simulations of 16 models
170 that participating in the Coupled Model Intercomparison Project Phase 5 (CMIP5)
171 (Table S2). We recalculated the RCP8.5 outputs as the following.

$$172 \quad V_{\text{new}}(i) = \overline{RCP8.5}_{2081-2100} - \overline{Hist}_{1981-2000} + V_{\text{Qian}}(i) \quad , \quad i = 1982, 1982, K \ 2000$$

173 where $\overline{RCP8.5}_{2081-2100}$ and $\overline{Hist}_{1981-2000}$ are the 20-year averages for the period 2081–
174 2100 in CMIP5 RCP8.5 simulations and the period 1981–2000 in CMIP5 historical
175 simulations, respectively. Their differences mean the future climate changes predicted
176 by each CMIP5 model. By adding these differences to the present-day forcing data (
177 V_{Qian}), we finally derived the new future forcing datasets (V_{new}). This method can
178 reduce the dependence on CMIP5 models and the uncertainties in future forcing
179 datasets and is comparable to the present-day forcing data from Qian et al. (2006).

180 This study conducted a few simulations, including the spin-up simulation (Fig.
181 S2). We first drove IAP-DGVM from bare ground for 660 model years to approach an
182 equilibrium state by cycling the atmospheric forcing data during the period 1972–
183 2004 from Qian et al. (2006). Then, we further conducted two sets of simulations, the
184 present-day simulation (hereafter Pre) and the future simulation (hereafter RCP8.5).
185 The Pre simulation was forced by the atmospheric data during 1972–2004 from Qian
186 et al. (2006) and ran for 33 model years, while the RCP8.5 simulations were forced by
187 the recalculated datasets described above and ran for 600 model years to approach
188 another equilibrium state. We compared the results between the Pre simulation for the
189 period 1981–2000 and the RCP8.5 simulations for the period 2081–2100. To
190 investigate the effects of climate factors on vegetation dynamics, we fixed
191 atmospheric CO₂ concentration at a constant value of 367.00 ppm in all simulations to
192 isolate the effects of CO₂ fertilization. All the simulations were run with a T85
193 resolution (128 × 256 grid cells). Finally, we obtained future changes in vegetation
194 distribution and carbon fluxes from the differences among the results of one present-
195 day simulation and 16 RCP8.5 simulations. To reduce the effects of cropland, we
196 weighted the vegetation coverage by a factor of (100%–FC_{crop}) in each grid cell,
197 where FC_{crop} represents the fractional coverage of crops (Zeng et al., 2014).

198 **3. Results**

199 ***3.1. Surface climate change***

200 The projected future land surface shows an overall warm and wet change relative
201 to the present day (Fig. 1). Globally, the annual mean surface air temperature in the
202 future is 4.87 ± 1.14 K higher than that in the present day. The positive temperature
203 anomalies are stronger over northern high latitudes than in other regions and are
204 projected by all 16 selected models (Fig. 1a). Meanwhile, the projected global mean
205 precipitation is 0.45 ± 0.07 mm day⁻¹ higher than that in the present day. The positive
206 precipitation anomalies are more pronounced in several regions, such as western and
207 eastern North America, Europe, northeast and southeast Asia, equatorial Africa, and
208 southern South America. However, negative precipitation anomalies are seen over
209 Amazon, the region showing larger uncertainties in the projected precipitation among
210 models than other regions (Fig. 1b). These climate anomalies are qualitatively
211 consistent with a large body of published studies that reported future predictions of
212 global warming and the possible drying of tropical regions in the future (Yu et al.,
213 2014; Yin et al., 2018; Tømmervik and Forbes, 2020; Wibowo et al., 2020).

214 **3.2. *Vegetation distribution***

215 We first analyzed the changes in vegetation distributions for the four aggregated
216 vegetation types (trees, shrubs, grasses and bare ground) between the RCP8.5
217 experiments and the present-day experiment. In general, there is a greening anomaly
218 in the middle and high latitudes of the northern hemisphere (30°N–90°N) with
219 10.10% more projected vegetation. Trees and grasses contribute the most to the
220 positive anomaly, while shrubs show a negative anomaly (Table 1). In contrast, there
221 is a slight negative anomaly in the tropics (30°S–30°N) with 3.72% less projected

222 vegetation. Grasses and shrubs contribute the most to the negative anomaly, while
223 trees show almost no changes (Table 1).

224 Figure 2 shows a poleward expansion of the projected vegetation. The
225 vegetation-growing regions in the RCP8.5 experiments are farther north than those in
226 the present-day experiment, with 10°, 5° and 7° for trees, shrubs and grasses,
227 respectively. The spatial distribution shows that the poleward expansion mainly
228 occurred in northern Canada and Siberia for trees and grasses and in northeastern
229 Canada for shrubs (Fig. S3). These results are qualitatively consistent with previous
230 studies based on other multiple GCMs (Alo and Wang, 2008; Yu et al., 2014; Gang et
231 al., 2017) and with some observation-based studies (Speed et al., 2010; Vickers et al.,
232 2016), indicating a poleward expansion of vegetation over mid-high latitudes in the
233 future.

234 The changes in vegetation distribution can be seen more directly by an estimation
235 of the differences in the four aggregated vegetation between the two scenarios (Fig.
236 2). Over northern mid-high latitudes, the increase in trees in the RCP8.5 experiments
237 is mainly in Alaska, eastern Canada and Siberia. However, a decrease in trees is also
238 seen in central Canada, Western Siberia, and Northeast China. The decreased shrubs
239 mainly occurred in northwestern Canada, western America and eastern Siberia and are
240 correspondingly replaced by the increased grasses. Over the tropics, the decreased
241 grasses and shrubs shown in Figure 2 mainly occurred in tropical Africa and
242 Australia, with 8.57% and 3.00%, respectively. Trees in tropical America decreased
243 by 4.89%, even though the whole tropical trees showed almost no changes. Figure 2

244 also illustrates that the changes in the projected vegetation in above mentioned
245 regions are consistent among the selected 16 models.

246 To figure out the contribution of each PFT to the four aggregated vegetation, we
247 further compared the fractional coverage of vegetation at the PFT level in the two
248 scenarios (Fig. 3). The increased trees shown in Figure 2 are dominantly contributed
249 by “broadleaf deciduous temperate tree” (BDM; 3.37%), while “needleleaf evergreen
250 boreal tree” (NEB) makes the largest negative contribution with a decrease by 1.13%.
251 The decreased shrubs in the future are dominated by the decreased “broadleaf
252 deciduous boreal shrub” (BDBsh; -5.18%). For the increased grasses, positive
253 contributions are mainly from “C3 arctic grass” (C3Ar; 3.74%) and “C3 non-arctic
254 grass” (C3NA; 4.17%), but “C4 grass” (C4) makes a negative contribution with
255 2.01%. The six mentioned PFTs show the largest sensitivities to the global warming
256 and are the main contributors to the global vegetation changes.

257 **3.3. LAI**

258 Over the whole globe, the projected LAI in the RCP8.5 experiments increased by
259 $0.65 \pm 0.30 \text{ m}^2 \text{ m}^{-2}$, relative to the present-day experiment. This increase is seen over
260 most latitudes, especially in the middle and high latitudes (Fig. 4b). Figure 4a shows
261 the spatial pattern of the differences in LAI between the RCP8.5 experiments and the
262 present-day experiment. Over northern mid-high latitudes, the increased LAI mainly
263 occurred in Alaska, eastern Canada, central North America, and eastern Siberia, with
264 more than $2.00 \text{ m}^2 \text{ m}^{-2}$. However, a strong decrease in LAI is also seen in central
265 Canada, Western Siberia, and Northeast China, the regions showing the projected

266 replacement of trees and shrubs by grasses (Fig. 2). Over the tropics, the projected
267 LAI decreased in Amazon and equatorial Africa by exceeding $1.00 \text{ m}^2 \text{ m}^{-2}$, while
268 southeastern Asia showed an increase in the projected LAI by more than $1.00 \text{ m}^2 \text{ m}^{-2}$.

269 **3.4. Carbon fluxes**

270 The analysis here focuses on the changes of carbon fluxes for GPP, NPP and
271 autotrophic respiration (R_a) between the RCP8.5 experiments and the present-day
272 experiment. Globally, positive anomalies were observed for all the three carbon fluxes
273 (Fig. 5). GPP shows the largest anomaly with $18.36 \pm 5.52\%$, which is followed by R_a
274 and NPP, with $12.32 \pm 3.24\%$ and $6.04 \pm 2.42\%$, respectively. Considering that the
275 CO_2 concentration is same in all simulations, the overall positive anomalies in GPP
276 and NPP are caused by the warmer and wetter climate in the future, a favorable
277 climatic condition that can enhance photosynthesis by lengthening the growing season
278 or by reducing water limitation. Further analysis is shown in Section 4.

279 Figure 6 clearly shows that the positive anomalies occurred over most of the
280 latitudes, while negative anomalies were seen over a few tropical latitudes. The spatial
281 patterns further show that the positive anomalies are more globally widespread than
282 the negative anomalies (Fig. 6a, Fig. 6c and Fig. 6e). Over middle and high latitudes,
283 the regions with remarkable positive anomalies are mainly in Alaska, eastern North
284 America, Europe, eastern Siberia, and southern South America. Regions with negative
285 or slightly positive anomalies are seen in Northeast China and Western Siberia. Over
286 the tropics, the negative anomalies of the three carbon fluxes are observed mainly in
287 Amazon, while tropical Asia shows remarkable positive anomalies. Figure 6 also

288 illustrates that the projected positive anomalies are more consistent than the projected
289 negative anomalies among the 16 RCP8.5 experiments, which reflects more
290 uncertainties in the projected carbon fluxes over regions with negative changes.

291 **4. Discussion**

292 *4.1. Linkage between climate and vegetation anomalies*

293 To investigate drivers of the changes in vegetation distribution, we further
294 analyzed the relationships between the changes in fractional coverage (FC) of the
295 above mentioned six PFTs and temperature, precipitation, respectively (Fig. 7). The
296 changes in temperature are significantly and negatively correlated with the changes in
297 “needleleaf evergreen boreal tree” (NEB), “broadleaf deciduous boreal shrub”
298 (BDBsh) and “C4 grass” (C4), with correlation coefficients (cc) of -0.89 , -0.65 and $-$
299 0.51 , respectively. In contrast, significantly positive correlations are seen between the
300 changes in temperature and “broadleaf deciduous temperate tree” (BDM; $cc=0.88$),
301 “C3 arctic grass” (C3Ar; $cc=0.85$) and “C3 non-arctic grass” (C3NA; $cc=0.64$).
302 Figure 7b shows that the changes in precipitation are significantly correlated with the
303 changes in NEB ($cc=-0.48$), BDBsh ($cc=-0.60$), and C3Ar ($cc=0.63$), while the
304 correlations for the other three PFTs are not significant. Together with the partial
305 correlation coefficients (Table S3), the stronger correlations between fractional
306 coverage of vegetation and surface air temperature indicate that temperature is the
307 dominant driver of the changes in vegetation distribution relative to precipitation.

308 The dominant role of surface air temperature in driving vegetation distribution
309 reflects that temperature is a key limiting factor for vegetation growth. The warmer
310 climate in the future can lead to an expansion of the growing season and increased
311 photosynthesis rates in the boreal and temperate regions. High temperatures also lead
312 to higher mortality rates for boreal woods (NEB and BDBsh) due to heat stress and
313 thus a decrease in FC. However, the heat stress is neglected in DGVMs for temperate
314 vegetation which is adjusted to the warm climate, and thus results in an increase in FC
315 for BDM and C3 grasses. For C4 grass that grows in the tropics (Fig. S4), warming
316 has little or even negative impacts on the rate of photosynthesis but significantly
317 increases the rate of respiration, thus suppresses productivity and leads to a decreased
318 FC.

319 We next investigate the relationship between projected changes in the three
320 carbon fluxes and changes in LAI, surface air temperature, and precipitation. The
321 three carbon fluxes are known to be impacted greatly by LAI, temperature, and
322 precipitation. Their net effects can be very different in different ecosystems, so the
323 changes in the three carbon fluxes show large differences. Thus, we selected six
324 regions (Table S4) to discuss these differences by using region boundaries defined in
325 previous studies (Giorgi and Francisco, 2000; Xue et al., 2010). In these regions, the
326 projected changes in the three carbon fluxes are either remarkably increased, slightly
327 increased, or decreased (Fig. S5).

328 Over northern mid-high latitudes, it is known that an increase in LAI,
329 temperature, and precipitation is generally favorable for an increase in GPP, NPP, and

330 Ra. Figure 8 shows a remarkable increase in the projected carbon fluxes in Alaska
331 (ALA), Northern Europe (NEU), and eastern North America (ENA). The increases
332 are positively contributed by combined effects resulting from increases in LAI,
333 temperature, and precipitation. However, in Western Siberia (WSI), the replacement
334 of trees and shrubs by grasses (Fig. S6) leads to a decrease in LAI and in the carbon
335 fluxes, which partly offsets the increase in the carbon fluxes caused by the increased
336 temperature and precipitation. The net result ultimately leads to a slight increment of
337 the carbon fluxes by no more than 0.50 PgC yr^{-1} in WSI.

338 Over the tropics, warmer climate anomalies may reduce vegetation productivity
339 due to a suppression of photosynthesis caused by a higher vapor pressure deficit,
340 while wetter climate anomalies can enhance vegetation productivity by reducing
341 water stress. Figure 8 shows weaker positive anomalies in the projected temperature
342 and stronger positive anomalies in the projected precipitation in Southeast Asia (SEA)
343 than in the Amazon Basin (AMZ). These differences, on one hand, explain the
344 opposite responses in the carbon fluxes in the two regions. On the other hand, the
345 increased LAI caused by increased trees in SEA also makes large contributions to the
346 enhanced carbon fluxes, while the decreased LAI caused by decreased trees in AMZ
347 makes large contributions to the decreased carbon fluxes. Overall, the combination of
348 the effects caused by LAI, temperature and precipitation results in the opposite
349 behaviors of SEA and AMZ on the responses of carbon fluxes.

350 ***4.2. Uncertainties and significance***

351 This work mainly focuses on the impact of climate warming on vegetation
352 dynamics and carbon fluxes, so the atmospheric CO₂ concentration is kept at a
353 constant value in all simulations to isolate CO₂ fertilization effects. This set may
354 influence our full understanding of vegetation responses. Thus, we further conducted
355 a simulation with an elevated CO₂ of 850 ppm (hereafter eCO₂) by referring to Yu et
356 al. (2014). We compared the results with the above results to discuss the differences
357 in the effects of global warming and CO₂ fertilization on vegetation dynamics and
358 carbon fluxes.

359 The results show that the eCO₂ simulation also produced more vegetation than
360 the Pre simulation. The value of the greening anomaly is comparable to that of the
361 RCP8.5 simulation (Fig. S7). However, there is no poleward expansion of vegetation
362 in the eCO₂ simulation over the northern high latitudes (Fig. S8). The three carbon
363 fluxes are also enhanced in the eCO₂ simulation relative to the Pre simulation. Their
364 global annual totals are comparable to those in the RCP8.5 simulation (Fig. S9). The
365 spatial distribution shows that the enhancement of the three carbon fluxes of the eCO₂
366 simulation is seen over almost all vegetated land grids (Fig. S10), while the RCP8.5
367 simulation shows a negative anomaly in the three carbon fluxes over more vegetated
368 grids (Fig. 6). The comparable results between the RCP8.5 and eCO₂ simulations
369 illustrate that the effects of global warming on vegetation dynamics and carbon fluxes
370 are as important as those of CO₂ fertilization.

371 Furthermore, in our study, the projected results were based on the forcing from
372 the RCP8.5 scenario, which corresponds to a very high baseline emission scenario to

373 maximize the climate signal (Taylor et al., 2012). Liu et al. (2020) assessed the future
374 changes in the climate-vegetation system over East Asia under different emission
375 scenarios. They found a slight increase in vegetation cover over most of the region
376 and the magnitude of these changes increased gradually from low to high RCPs. Thus,
377 more simulations and analyses are needed to investigate the dependence of the results
378 on the scenarios at the global scale.

379 Despite the uncertainties mentioned above, our study provides valuable
380 contributions to the development of the model and to understanding the responses of
381 vegetation to global warming. First, the results show the opposite response to
382 warming between “needleleaf evergreen boreal tree” (NEB) and “broadleaf deciduous
383 temperate tree” (BDM) due to the different sets for heat stress in the model. This
384 phenomenon reveals that the differences in parameters assigned to PFTs have
385 significantly different effects on the vegetation in response to future climate changes.
386 Meanwhile, this phenomenon reminds us that it is necessary to further improve the
387 parameterization of heat stress in IAP-DGVM because of the limitation of the sets.
388 Thus, optimizing the parameterization of vegetation processes in the model is crucial
389 for simulating a more realistic vegetation change. Second, this study provides a case
390 that shows an application of CAS-ESM2, studying the response of vegetation
391 dynamic to climate change. In the process of developing IAP-DGVM, the application
392 is a new stage after the successful coupling of IAP-DGVM with CAS-ESM2, and
393 provides a valuable sample for comparison with both the CAS-ESM2 community and
394 other model communities. We now have coupled IAP-DGVM with the atmospheric

395 general circulation model (IAP-AGCM; Zhang et al., 2013), so CAS-ESM2 can be
396 used to investigate interactions between vegetation dynamic and climate. We now use
397 this coupled version of CAS-ESM2 to run the Diagnostic, Evaluation and
398 Characterization of Klima (DECK) experiments of phase 6 of the Coupled Model
399 Intercomparison Project (CMIP6). Third, the poleward expansion of vegetation in
400 northern mid-high latitudes simulated in our work is consistent with numerous studies
401 on future projections (Mahowald et al., 2016; Yu et al., 2016; Gang et al., 2017;
402 Tharammal et al., 2018) and with recent observations (Zhu et al., 2016; Zeng et al.,
403 2018; Yao et al., 2019), indicating that the “greening” trend may continue in the
404 future. This greening can make critical feedbacks to the local climate by shading,
405 changing surface albedo and regulating the portion of evapotranspiration between
406 evaporation and transpiration (Blok et al., 2010; Zhu and Zeng, 2015, 2017). Our
407 investigation shows the dominant role of surface air temperature in this greening
408 phenomenon. The investigation is favorable for a better understanding of vegetation
409 processes and for further knowledge of the model behavior in response to global
410 warming, which favors projections of changes in terrestrial ecosystems and climate in
411 the future. Overall, this work evaluates the responses of vegetation to global warming
412 and shows the tight linkage between vegetation and climate changes, which is a
413 necessary step for model development and a significant foundation for further study
414 of vegetation-climate interactions.

415 **5. Summary**

416 This study investigated the changes in vegetation distribution and carbon fluxes
417 in response to global warming by using IAP-DGVM in CAS-ESM2. The results based
418 on the present-day simulation and RCP8.5 simulations showed a greening in the
419 northern middle and high latitudes and a slight browning in the tropics. The results
420 also showed positive anomalies in GPP, NPP, and Ra over most latitudes, while
421 negative anomalies occurred in Amazon. We argued that surface air temperature is the
422 dominant driver of the changes in vegetation distribution relative to precipitation and
423 the changes in GPP, NPP, and Ra can be explained by the combined effects of LAI,
424 temperature and precipitation. Our results show the application of CAS-ESM2 by
425 simulating the response of terrestrial ecosystems to global warming and by
426 investigating the underlying mechanisms. The investigation is favorable for a better
427 understanding of vegetation processes and for a further improvement in the model
428 parameterizations.

429 **Acknowledgments.** This work was supported by the National Natural Science
430 Foundation of China (Grant Number 41705070) and the Major Program
431 of the National Natural Science Foundation of China (Grant Number 41991282).

432

433 REFERENCES

434 Alo, C. A., and G. L. Wang, 2008: Potential future changes of the terrestrial
435 ecosystem based on climate projections by eight general circulation models.
436 *Journal of Geophysical Research*, **113**, <https://doi.org/10.1029/2007JG000528>.

437 Anav, A., and Coauthors, 2015: Spatiotemporal patterns of terrestrial gross primary
438 production: A review. *Reviews of Geophysics*, **53**(3), 785–818,
439 <https://doi.org/10.1002/2015RG000483>.

440 Andreu-Hayles, L., R. D'Arrigo, K. J. Anchukaitis, P. S. A. Beck, D. Frank, and S.
441 Goetz, 2011: Varying boreal forest response to arctic environmental change at
442 the Firth River, Alaska. *Environmental Research Letters*, **6**(4),
443 <https://doi.org/0.1088/1748-9326/6/4/045503>.

444 Arora, V. K., and Coauthors, 2020: Carbon-concentration and carbon-climate
445 feedbacks in CMIP6 models and their comparison to CMIP5 models.
446 *Biogeosciences*, **17**(16), 4173–4222, <https://doi.org/10.5194/bg-2019-473>.

447 Bi, J., L. Xu, A. Samanta, Z. C. Zhu, and R. Myneni, 2013: Divergent Arctic-boreal
448 vegetation changes between North America and Eurasia over the past 30 years.
449 *Remote Sensing*, **5**(5), 2093–2112, <https://doi.org/10.3390/rs5052093>.

450 Blok, D., M. M. P. D. Heijmans, G. Schaepman-Strub, A. V. Kononov, T. C.
451 Maximov, and F. Berendse, 2010: Shrub expansion may reduce summer
452 permafrost thaw in Siberian tundra. *Global Change Biology*, **16**(4), 1296–1305,
453 <https://doi.org/10.1111/j.1365-2486.2009.02110.x>.

454 Brovkin, V., T. Raddatz, C. H. Reick, M. Claussen, and V. Gayler, 2009: Global
455 biogeophysical interactions between forest and climate. *Geophysical Research*
456 *Letters*, **36**(7), <https://doi.org/10.1029/2009GL037543>.

457 Cao, X. Y., F. Tian, A. Dallmeyer, and U. Herzschuh, 2019: Northern hemisphere
458 biome changes (>30°N) since 40 cal ka BP and their driving factors inferred

459 from model-data comparisons. *Quaternary Science Reviews*, **220**, 291–309,
460 <https://doi.org/10.1016/j.quascirev.2019.07.034>.

461 Clark, D. A., S. C. Piper, C. D. Keeling, and D. B. Clark, 2003: Tropical rain forest
462 tree growth and atmospheric carbon dynamics linked to interannual temperature
463 variation during 1984–2000. *Proceedings of the National Academy of Sciences*,
464 **100**(10), 5852–5857, <https://doi.org/10.1073/pnas.0935903100>.

465 Corlett, R. T., 2011: Impacts of warming on tropical lowland rainforests. *Trends in*
466 *Ecology and Evolution*, **26**(11), 606–613,
467 <https://doi.org/10.1016/j.tree.2011.06.015>.

468 Cramer, W., and Coauthors, 2001: Global response of terrestrial ecosystem structure
469 and function to CO₂ and climate change: results from six dynamic global
470 vegetation models. *Global Change Biology*, **7**(4), 357–373,
471 <https://doi.org/10.1046/j.1365-2486.2001.00383.x>.

472 De Kauwe, M. G., and Coauthors, 2014: Where does the carbon go? A model-data
473 intercomparison of vegetation carbon allocation and turnover processes at two
474 temperate forest free-air CO₂ enrichment sites. *New Phytologist*, **203**(3), 883–
475 899, <https://doi.org/10.1111/nph.12847>.

476 Diffenbaugh, N. S., and C. B. Field, 2013: Changes in ecologically critical
477 terrestrial climate conditions. *Science*, **341**(6145), 486–492,
478 <https://doi.org/10.1126/science.1237123>.

479 Doughty, C. E., and M. L. Goulden, 2008: Are tropical forests near a high temperature
480 threshold? *Journal of Geophysical Research: Biogeosciences*, **113**,

481 <https://doi.org/10.1029/2007JG000632>.

482 Eric, D. M., D. A. Galvao, and D. A. Way, 2018: Plant carbon metabolism and
483 climate change: elevated CO₂ and temperature impacts on photosynthesis,
484 photorespiration and respiration. *New Phytologist*, **221**,
485 <https://doi.org/10.1111/nph.15283>.

486 Falloon, P. D., R. Dankers, R. A. Betts, C. D. Jones, B. B. B. Booth, and F. H.
487 Lambert, 2012: Role of vegetation change in future climate under the A1B
488 scenario and a climate stabilisation scenario, using the HadCM3C Earth system
489 model. *Biogeosciences*, **9**(11), 4739–4756, [https://doi.org/10.5194/bg-9-4739-](https://doi.org/10.5194/bg-9-4739-2012)
490 2012.

491 Fan, Z. M., and B. Fan, 2019: Shifts of the mean centers of potential vegetation
492 ecosystems under future climate change in Eurasia. *Forests*, **10**(10),
493 <https://doi.org/10.3390/f10100873>.

494 Field, C. B., L. D. Mortsch, M. Brklacich, D. L. Forbes, P. Kovacs, J. A. Patz, S. W.
495 Running, and M. J. Scott, 2007: North America. Climate change 2007: Impacts,
496 Adaptation and Vulnerability. Contribution of Working Group II to the Third
497 Assessment Report, **19**(2), 81–111, [https://doi.org/10.9774/GLEAF.978-1-](https://doi.org/10.9774/GLEAF.978-1-907643-29-3_4)
498 907643-29-3_4.

499 Fraser, R. H., I. Olthof, M. Carriere, A. Deschamps, and D. Pouliot, 2011: Detecting
500 long-term changes to vegetation in northern Canada using the Landsat satellite
501 image archive. *Environmental Research Letters*, **6**, [https://doi.org/10.1088/1748-](https://doi.org/10.1088/1748-9326/6/4/045502)
502 9326/6/4/045502.

503 Frost, G. V., and H. E. Epstein, 2014: Tall shrub and tree expansion in Siberian tundra
504 ecotones since the 1960s. *Global Change Biology*, **20**(4), 1264–1277,
505 <https://doi.org/10.1111/gcb.12406>.

506 Gang, C. C., Y. Z. Zhang, Z. Q. Wang, Y. Z. Chen, Y. Yang, J. L. Li, J. M. Cheng, J.
507 G. Qi, and I. Odeh, 2017: Modeling the dynamics of distribution, extent, and
508 NPP of global terrestrial ecosystems in response to future climate change. *Global
509 and Planetary Change*, **148**, 153–165,
510 <https://doi.org/10.1016/j.gloplacha.2016.12.007>.

511 Gao, D. D., L. Dan, G. Z. Fan, J. Peng, X. J. Yang, F. Q. Yang, and Y. Y. Li, 2019:
512 Spatial and Temporal Variations of Net Primary Productivity at Century Scale in
513 Earth System Models and Its Relationship with Climate. *Climatic and
514 Environmental Research*, **24**(6), 663–677, <https://doi.org/10.3878/j.issn.1006-9585.2018.18052>. (in Chinese)

516 Giorgi, F., R. Francisco, 2000: Uncertainties in regional climate change prediction: a
517 regional analysis of ensemble simulations with the HADCM2 coupled AOGCM.
518 *Climate Dynamics*, **16**(2), 169–182, <https://doi.org/10.1007/PL00013733>.

519 Gurney, K. R., and Coauthors, 2004: Transcom 3 inversion intercomparison: Model
520 mean results for the estimation of seasonal carbon sources and sinks. *Global
521 Biogeochemical Cycles*, **18**, 95–110, <https://doi.org/10.1029/2003GB002111>.

522 Hawkins, L. R., and Coauthors, 2019: Parametric sensitivity of vegetation dynamics
523 in the TRIFFID model and the associated uncertainty in projected climate change
524 impacts on Western US forests. *Journal of Advances in Modeling Earth Systems*,

525 11(8), 2787–2813, <https://doi.org/10.1029/2018MS001577>.

526 Horvath, P., and Coauthors, 2021: Improving the representation of high-latitude
527 vegetation distribution in dynamic global vegetation models. *Biogeosciences*,
528 18(1), 95–112, <https://doi.org/10.5194/bg-18-95-2021>.

529 Hu, L., W. J. Fan, W. P. Yuan, H. Z. Ren, and Y. K. Cui, 2021: Spatiotemporal
530 variation of vegetation productivity and its feedback to climate change in
531 northeast china over the last 30 years. *Remote Sensing*, 13(5), 951,
532 <https://doi.org/10.3390/rs13050951>.

533 Huang, M. T., and Coauthors, 2019: Air temperature optima of vegetation
534 productivity across global biomes. *Nature Ecology & Evolution*, 3(5), 772–779,
535 <https://doi.org/10.1038/s41559-019-0838-x>.

536 Jung, M., and Coauthors, 2007: Uncertainties of modeling gross primary productivity
537 over Europe: A systematic study on the effects of using different drivers and
538 terrestrial biosphere models. *Global Biogeochemical Cycles*, 21(4),
539 <https://doi.org/10.1029/2006GB002915>.

540 Keenan, T. F., and W. J. Riley, 2018: Greening of the land surface in the world's cold
541 regions consistent with recent warming. *Nature Climate Change*, <https://doi.org/10.1038/s41558-018-0258-y>.

542

543 Knorr, W., and M. Heimann, 2001: Uncertainties in global terrestrial biosphere
544 modeling: 1. A comprehensive sensitivity analysis with a new photosynthesis
545 and energy balance scheme. *Global Biogeochemical Cycles*, 15(1), 207–225,
546 <https://doi.org/10.1029/1998GB001059>.

547 Kreplin, H. N., C. S. S. Ferreira, G. Destouni, S. D. Keesstra, L. Salvati, and Z.
548 Kalantari, 2021: Arctic wetland system dynamics under climate warming. *Wiley*
549 *Interdisciplinary Reviews-Water*, **8**(4), <https://doi.org/10.1002/wat2.1526>.

550 Kumar, D., and S. Scheiter, 2019: Biome diversity in South Asia—How can we
551 improve vegetation models to understand global change impact at regional level?
552 *Science of the Total Environment*, **671**, 1001–1016,
553 <https://doi.org/10.1016/j.scitotenv.2019.03.251>.

554 Li, F., X. D. Zeng, and S. Levis, 2012: A process-based fire parameterization of
555 intermediate complexity in a Dynamic Global Vegetation Model.
556 *Biogeosciences*, **9**(11), 4771–4772, <https://doi.org/10.5194/bg-9-4771-2012>.

557 Liu, L. B., and Coauthors, 2018: Broad consistency between satellite and vegetation
558 model estimates of net primary productivity across global and regional scales.
559 *Journal of Geophysical Research: Biogeosciences*, **123**(12), 3603–3616,
560 <https://doi.org/10.1029/2018JG004760>.

561 Liu, W. G., G. L. Wang, M. Yu, H. S. Chen, Y. L. Jiang, M. J. Yang, and Y. Shi,
562 2020: Projecting the future vegetation-climate system over East Asia and its
563 RCP-dependence. *Climate Dynamics*, **55**(9), 2725–2742,
564 <https://doi.org/10.1007/s00382-020-05411-2>.

565 Liu, Y., Y. K. Xue, G. MacDonald, P. Cox, and Z. Q. Zhang, 2019: Global vegetation
566 variability and its response to elevated CO₂, global warming, and climate
567 variability—a study using the offline SSiB4/TRIFFID model and satellite data.
568 *Earth System Dynamics*, **10**(1), 9–29, <https://doi.org/10.5194/esd-10-9-2019>.

569 Mackay, A., 2007: Climate change 2007: Impacts, Adaptation and Vulnerability.
570 Contribution of Working Group II to the Fourth Assessment Report of the
571 Intergovernmental Panel on Climate Change. *Journal of Environmental Quality*,
572 **37**(6), <https://doi.org/10.2134/jeq2008.0015br>.

573 Madani, N., and Coauthors, 2020: Recent amplified global gross primary productivity
574 due to temperature increase is offset by reduced productivity due to water
575 constraints. *AGU Advances*, **1**(4), <https://doi.org/10.1029/2020AV000180>.

576 Mahowald, N., F. Lo, Y. Zheng, L. Harrison, C. Funk, D. Lombardozzi, and C.
577 Goodale, 2016: Projections of leaf area index in earth system models. *Earth*
578 *System Dynamics*, **7**(1), 211–229, <https://doi.org/10.5194/esd-7-211-2016>.

579 Mao, J. F., and Coauthors, 2016: Human-induced greening of the northern
580 extratropical land surface. *Nature Climate Change*, **6**(10),
581 <https://doi.org/10.1038/nclimate3056>.

582 McGuire, A. D., and Coauthors, 2001: Carbon balance of the terrestrial biosphere in
583 the twentieth century: Analyses of CO₂, climate and land use effects with four
584 process-based ecosystem models. *Global Biogeochemical Cycles*, **15**(1), 183–
585 206, <https://doi.org/10.1029/2000gb001298>.

586 Mekonnen, Z. A., and Coauthors, 2021: Arctic tundra shrubification: a review of
587 mechanisms and impacts on ecosystem carbon balance. *Environmental Research*
588 *Letters*, **16**(5), <https://doi.org/10.1088/1748-9326/abf28b>.

589 Myers-Smith, I. H., and Coauthors, 2011: Shrub expansion in tundra ecosystems:
590 dynamics, impacts and research priorities. *Environmental Research Letters*, **6**(4),

591 <https://doi.org/10.1088/1748-9326/6/4/045509>.

592 Myers-Smith, I. H., and Coauthors, 2020: Complexity revealed in the greening of the
593 Arctic. *Nature Climate Change*, **10**(2), 106–117, [https://doi.org/10.1038/s41558-](https://doi.org/10.1038/s41558-019-0688-1)
594 019-0688-1.

595 Nemani, R. R., C. D. Keeling, H. Hashimoto, W. M. Jolly, S. C. Piper, C. J. Tucker,
596 R. B. Myneni, and S. W. Running, 2003: Climate-driven increases in global
597 terrestrial net primary production from 1982 to 1999. *Science*, **300**(5625), 1560–
598 1563, <https://doi.org/10.1126/science.1082750>.

599 Piao, S. L., and Coauthors, 2013: Evaluation of terrestrial carbon cycle models for
600 their response to climate variability and to CO₂ trends. *Global Change Biology*,
601 **19**(7), 2117–2132, <https://doi.org/10.1111/gcb.12187>.

602 Piao, S. L., P. Friedlingstein, P. Ciais, N. Viovy, and J. Demarty, 2007: Growing
603 season extension and its impact on terrestrial carbon cycle in the Northern
604 Hemisphere over the past 2 decades. *Global Biogeochemical Cycles*, **21**(3),
605 <https://doi.org/10.1029/2006GB002888>.

606 Piao, S. L., X. H. Wang, T. Park, C. Chen, X. Lian, Y. He, J. W. Bjerke, A. Chen, P.
607 Ciais, H. Tømmervik, R. R. Nemani, and R. B. Myneni, 2020: Characteristics,
608 drivers and feedbacks of global greening. *Nature Reviews Earth & Environment*,
609 **1**, 1–14, <https://doi.org/10.1038/s43017-019-0001-x>.

610 Prentice, I. C., A. Bondeau, W. Cramer, S. P. Harrison, T. Hickler, W. Lucht, S. Sitch,
611 B. Smith, and M. T. Sykes, 2007: Dynamic global vegetation modeling:
612 Quantifying terrestrial ecosystem responses to large-scale environmental change.

613 *Terrestrial Ecosystems in a Changing World*, J. G. Canadell, et al., Eds, The
614 IGBP Series, Springer-Verlag, Berlin, 175–192.

615 Qian, T. T., A. G. Dai, K. E. Trenberth, and K. W. Oleson, 2006: Simulation of global
616 land surface conditions from 1948 to 2004. Part I: Forcing data and evaluations.
617 *Journal of Hydrometeorology*, **7**(5), 953–975, [https://doi.org/10.1175/
618 JHM540.1](https://doi.org/10.1175/JHM540.1).

619 Quillet, A., C. H. Peng, and M. Garneau, 2010: Toward dynamic global vegetation
620 models for simulating vegetation-climate interactions and feedbacks: Recent
621 developments, limitations, and future challenges. *Environmental Reviews*, **18**,
622 333–353, <https://doi.org/10.1139/A10-016>.

623 Raddatz, T. J., C. H. Reick, W. Knorr, J. Kattge, E. Roeckner, R. Schnur, K. G.
624 Schnitzler, P. Wetzler, and J. Jungclaus, 2007: Will the tropical land biosphere
625 dominate the climate-carbon cycle feedback during the twenty-first century?
626 *Climate Dynamics*, **29**(6), 565–574, <https://doi.org/10.1007/s00382-007-0247-8>.

627 Schaphoff, S., C. P. O. Reyer, D. Schepaschenko, D. Gerten, and A. Shvidenko, 2016:
628 Tamm review: Observed and projected climate change impacts on Russia's
629 forests and its carbon balance. *Forest Ecology and Management*, **361**, 432–444,
630 <https://doi.org/10.1016/j.foreco.2015.11.043>.

631 Scheiter, S., L. Langan, and S. L. Higgins, 2013: Next-generation dynamic global
632 vegetation models: learning from community ecology. *NEW PHYTOL*, **198**(3),
633 957–969, <https://doi.org/10.1111/nph.12210>.

634 Scheiter, S., and Coauthors, 2020: Climate change promotes transitions to tall

635 evergreen vegetation in tropical Asia. *Global Change Biology*, **26**(9), 5106–
636 5124, <https://doi.org/10.1111/gcb.15217>.

637 Shafer, S. L., P. J. Bartlein, E. M. Gray, and R. T. Pellier, 2015: Projected future
638 vegetation changes for the Northwest United States and Southwest Canada at a
639 fine spatial resolution using a dynamic global vegetation model. *PloS one*,
640 **10**(10), <https://doi.org/10.1371/journal.pone.0138759>.

641 Shiyatov, S. G., M. M. Terent'ev, and V. V. Fomin, 2005: Spatiotemporal dynamics
642 of forest-tundra communities in the polar urals. *Russian Journal of Ecology*,
643 **36**(2), 69–75, <https://doi.org/10.1007/s11184-005-0051-9>.

644 Shevliakova, and Coauthors, 2020: The land component LM4.1 of the GFDL Earth
645 System Model ESM4.1: biophysical and biogeochemical processes and
646 interactions with climate. *J. Adv. Model. Earth Syst.*, (in review).

647 Sitch, S., and Coauthors, 2008: Evaluation of the terrestrial carbon cycle, future plant
648 geography and climate-carbon cycle feedbacks using five dynamic global
649 vegetation models (DGVMs). *GLOB CHANGE BIOL*, **14**(9), 2015–2039,
650 <https://doi.org/10.1111/j.1365-2486.2008.01626.x>.

651 Smith, B., D. Wärlind, A. Arneth, T. Hickler, P. Leadley, J. Siltberg, and S. Zaehle,
652 2014: Implications of incorporating N cycling and N limitations on primary
653 production in an individual-based dynamic vegetation model. *Biogeosciences*,
654 **11**(7), 2027–2054. <https://doi.org/10.5194/bg-11-2027-2014>.

655 Song, X., X. D. Zeng, J. W. Zhu, and P. Shao, 2016: Development of an
656 establishment scheme for a DGVM. *Adv. Atmos. Sci.*, **33**, 829–840,

657 <https://doi.org/10.1007/s00376-016-5284-y>.

658 Speed, J. D. M., S. J. Woodin, H. Tømmervi, and R. V. D. Wal, 2010: Extrapolating
659 herbivore-induced carbon loss across an arctic landscape. *Polar Biology*, **33**(6),
660 789–797, <https://doi.org/10.1007/s00300-009-0756-5>.

661 Sturm, M., C. Racine, and K. Tape, 2001: Climate change: increasing shrub
662 abundance in the Arctic. *Nature*, **411**(6837), 546–547,
663 <https://doi.org/10.1038/35079180>.

664 Suchul, K., and E. A. B. Eltahir, 2018: North China plain threatened by deadly
665 heatwaves due to climate change and irrigation. *Nature communications*, **9**,
666 <https://doi.org/10.1038/s41467-018-05252-y>.

667 Sulman, B. N., and Coauthors, 2019: Diverse mycorrhizal associations enhance
668 terrestrial C storage in a global model. *Global Biogeochemical Cycles*, **33**(4),
669 501–523, <https://doi.org/10.1029/2018GB005973>.

670 Taylor, K. E., R. J. Stouffer, and G. A. Meehl, 2012: An overview of CIMP5 and the
671 experiment design. *Bulletin of the American Meteorological Society*, **93**(4), 485–
672 498, <https://doi.org/10.1175/BAMS-D-11-00094.1>.

673 Tharammal T., G. Bala, D. Narayanappa, and R. Nemani, 2018: Potential roles of CO₂
674 fertilization, nitrogen deposition, climate change, and land use and land cover
675 change on the global terrestrial carbon uptake in the twenty-first century. *Climate
676 Dynamics*, **52**, 7–8, <https://doi.org/10.1007/s00382-018-4388-8>.

677 Tømmervik, H., and B. C. Forbes, 2020: Focus on recent, present and future Arctic
678 and boreal productivity and biomass changes. *Environ. Res. Lett*, **15**(8),

679 <https://doi.org/10.1088/1748-9326/ab79e3>.

680 Vickers, H., K. A. Hgda, S. Solb, S. R. Karlsen, H. Tømmervik, R. Aanes, and B. B.
681 Hansen, 2016: Changes in greening in the high arctic: insights from a 30 year
682 AVHRR max NDVI dataset for Svalbard. *Environmental Research Letters*,
683 **11**(10), <https://doi.org/10.1088/1748-9326/11/10/105004>.

684 Walker, M. D., and Coauthors, 2006: Plant community responses to experimental
685 warming across the tundra biome. *Proceedings of the National Academy of*
686 *Sciences*, **103**(5), 1342–1346, <https://doi.org/10.1073/pnas.0503198103>.

687 Wibowo, A., M. M. Yusoff, T. A. Adura, A. Wibowo, Supriatna, and L. H. Zaini,
688 2020: Spatial model of air surface temperature using Landsat 8 TIRS. *IOP*
689 *Conference Series: Earth and Environmental Science*, **500**,
690 <https://doi.org/10.1088/1755-1315/500/1/012009>.

691 Woodward, F. I., and B. G. Williams, 1987: Climate and plant distribution at global
692 and local scales. *Springer Netherlands*, **69**, 189–197,
693 <https://doi.org/10.1007/BF00038700>.

694 Woodward, F. I., and M. R. Lomas, 2004: Vegetation dynamics-simulating responses
695 to climatic change. *Biological Reviews*, **79**(3), 643–670,
696 <https://doi.org/10.1017/S1464793103006419>.

697 Wu, L., T. Kato, H. Sato, T. Hirano, and T. Yazaki, 2019: Sensitivity analysis of the
698 typhoon disturbance effect on forest dynamics and carbon balance in the future
699 in a cool-temperate forest in northern Japan by using SEIB-DGVM. *Forest*
700 *Ecology and Management*, **451**, <https://doi.org/10.1016/j.foreco.2019.117529>.

701 Xue, Y. K., F. D. Sales, R. Vasic, C. R. Mechoso, A. Arakawa, and S. Prince, 2010:
702 Global and seasonal assessment of interactions between climate and vegetation
703 biophysical processes: A GCM study with different land-vegetation
704 representations. *Journal of Climate*, **23**(23), 1411–1433,
705 <https://doi.org/10.1175/2009JCLI3054.1>.

706 Yao, R., L. C. Wang, X. Huang, X. X. Chen, and Z. J. Liu, 2019: Increased spatial
707 heterogeneity in vegetation greenness due to vegetation greening in mainland
708 China. *Ecological Indicators*, **99**, 240–250,
709 <https://doi.org/10.1016/j.ecolind.2018.12.039>.

710 Yin, Y. H., D. Y. Ma, and S. H. Wu, 2018: Climate change risk to forests in China
711 associated with warming. *Scientific Reports*, **8**, [https://doi.org/10.1038/s41598-](https://doi.org/10.1038/s41598-017-18798-6)
712 [017-18798-6](https://doi.org/10.1038/s41598-017-18798-6).

713 Yu, M., G. L. Wang, and H. S. Chen, 2016: Quantifying the impacts of land surface
714 schemes and dynamic vegetation on the model dependency of projected changes
715 in surface energy and water budgets. *Journal of Advances in Modeling Earth*
716 *Systems*, **8**(1), 370–386, <https://doi.org/10.1002/2015MS000492>.

717 Yu, M., G. L. Wang, D. Parr, and K. F. Ahmed, 2014: Future changes of the terrestrial
718 ecosystem based on a dynamic vegetation model driven with RCP8.5 climate
719 projections from 19 GCMs. *Climatic Change*, **127**(2), 257–271,
720 <https://doi.org/10.1007/s10584-014-1249-2>.

721 Yu, J. J., P. Berry, B. P. Guillod, and T. Hickler, 2021: Climate change impacts on the
722 future of forests in Great Britain. *Frontiers in Environmental Science*, **9**,

723 <https://doi.org/10.3389/fenvs.2021.640530>.

724 Zeng, X. D., X. B. Zeng, and M. Barlage, 2008: Growing temperate shrubs over arid
725 and semiarid regions in the community land model-dynamic global vegetation
726 model. *Global Biogeochemical Cycles*, **22**,
727 <https://doi.org/10.1029/2007GB003014>.

728 Zeng, X. D., 2010: Evaluating the dependence of vegetation on climate in an
729 improved dynamic global vegetation model. *ADVANCES IN ATMOSPHERIC*
730 *SCIENCES*, **27**(5), 977–991, <https://doi.org/10.1007/s00376-009-9186-0>.

731 Zeng, X. D., F. Li, and X. Song, 2014: Development of the IAP dynamic global
732 vegetation model. *Adv. Atmos. Sci.*, **31**, 505–514, [https://doi.org/10.1007/s00376-](https://doi.org/10.1007/s00376-013-3155-3)
733 [013-3155-3](https://doi.org/10.1007/s00376-013-3155-3).

734 Zeng, Z. Z., S. L. Piao, L. Z. X. Li, P. Ciais, Y. Li, X. T. Cai, L. Yang, M. F. Liu, and
735 E. F. Wood, 2018: Global terrestrial stilling: does Earth's greening play a role?
736 *Environmental Research Letters*, **13**(12), [https://doi.org/10.1088/1748-](https://doi.org/10.1088/1748-9326/aaca84)
737 [9326/aaca84](https://doi.org/10.1088/1748-9326/aaca84).

738 Zhang, H., M. H. Zhang, and Q. C. Zeng, 2013: Sensitivity of simulated climate to
739 two atmospheric models: Interpretation of differences between dry models and
740 moist models. *Monthly Weather Review*, **141**(5), 1558–1576,
741 <https://doi.org/10.1175/MWR-D-11-00367.1>.

742 Zhang, K., and Coauthors, 2015: The fate of Amazonian ecosystems over the coming
743 century arising from changes in climate, atmospheric CO₂ and land use. *Global*
744 *Change Biology*, **21**(7), 2569–2587, <https://doi.org/10.1111/gcb.12903>.

745 Zhang, H., and Coauthors, 2020: CAS-ESM2: Description and climate simulation
746 performance of the Chinese Academy of Sciences (CAS) Earth System Model
747 (ESM) Version 2. *Journal of Advances in Modeling Earth Systems*, **12**(12),
748 <https://doi.org/10.1029/2020MS002210>.

749 Zhu, J. W., and X. D. Zeng, 2015: Comprehensive study on the influence of
750 evapotranspiration and albedo on surface temperature related to changes in the
751 leaf area index. *Advances in Atmospheric Sciences*, **32**(7), 935–942,
752 <https://doi.org/10.1007/s00376-014-4045-z>.

753 Zhu, Z. C., and Coauthors, 2016: Greening of the Earth and its drivers. *Nature*
754 *Climate Change*, **6**(8), 791–795, <https://doi.org/10.1038/nclimate3004>.

755 Zhu, J. W., and X. D. Zeng, 2017: Influences of the seasonal growth of vegetation on
756 surface energy budgets over middle to high latitudes. *International Journal of*
757 *Climatology*, **37**(12), 4251–4260, <https://doi.org/10.1002/joc.5068>.

758 Zhu, J. W., M. H. Zhang, Y. Zhang, X. D. Zeng, and X. M. Xiao, 2018: Response of
759 tropical terrestrial gross primary production to the super El Niño event in 2015.
760 *Journal of Geophysical Research: Biogeosciences*, **123**(10), 3193–3203,
761 <https://doi.org/10.1029/2018JG004571>.

762 Zhu, J. W., X. D. Zeng, M. H. Zhang, Y. J. Dai, D. Y. Ji, F. Li, Q. Zhang, H. Zhang,
763 and X. Song, 2018: Evaluation of the new dynamic global vegetation model in
764 CAS-ESM. *Advances in Atmospheric Sciences*, **35**(6), 659–670,
765 <https://doi.org/10.1007/s00376-017-7154-7>.

766

767

768

769

770

771

772

773

774 **Table 1.** The changes of trees, shrubs and grasses between RCP8.5 experiments and

775 the present-day experiment in 30°N–90°N and 30°S–30°N, respectively.

	FC _{trees}	FC _{shrubs}	FC _{grasses}	FC _{total}
30°N–90°N	6.39%	–11.60%	15.31%	10.10%
30°S–30°N	0.002%	–1.26%	–2.46%	–3.72%

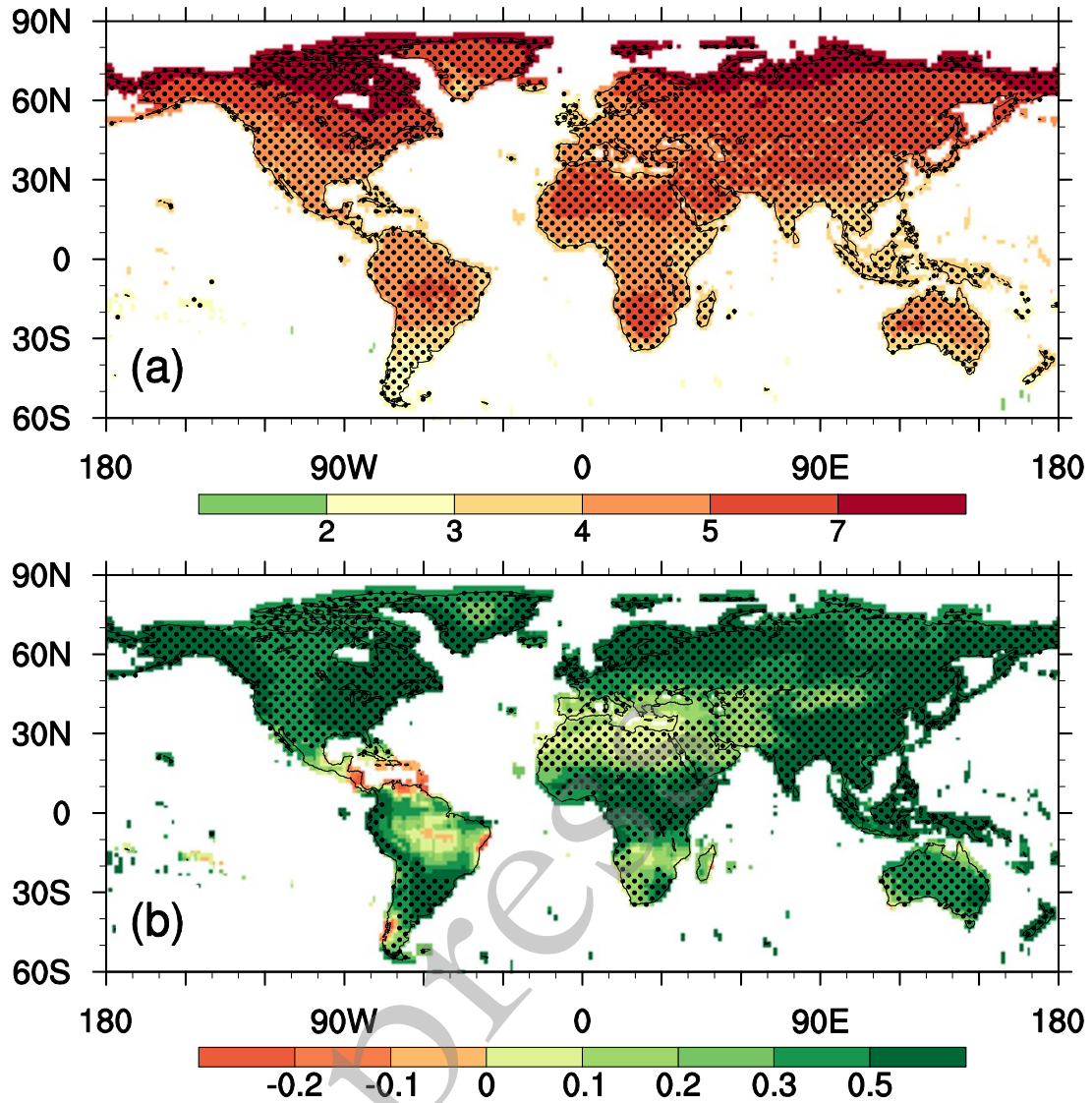
776

777

778

779

780



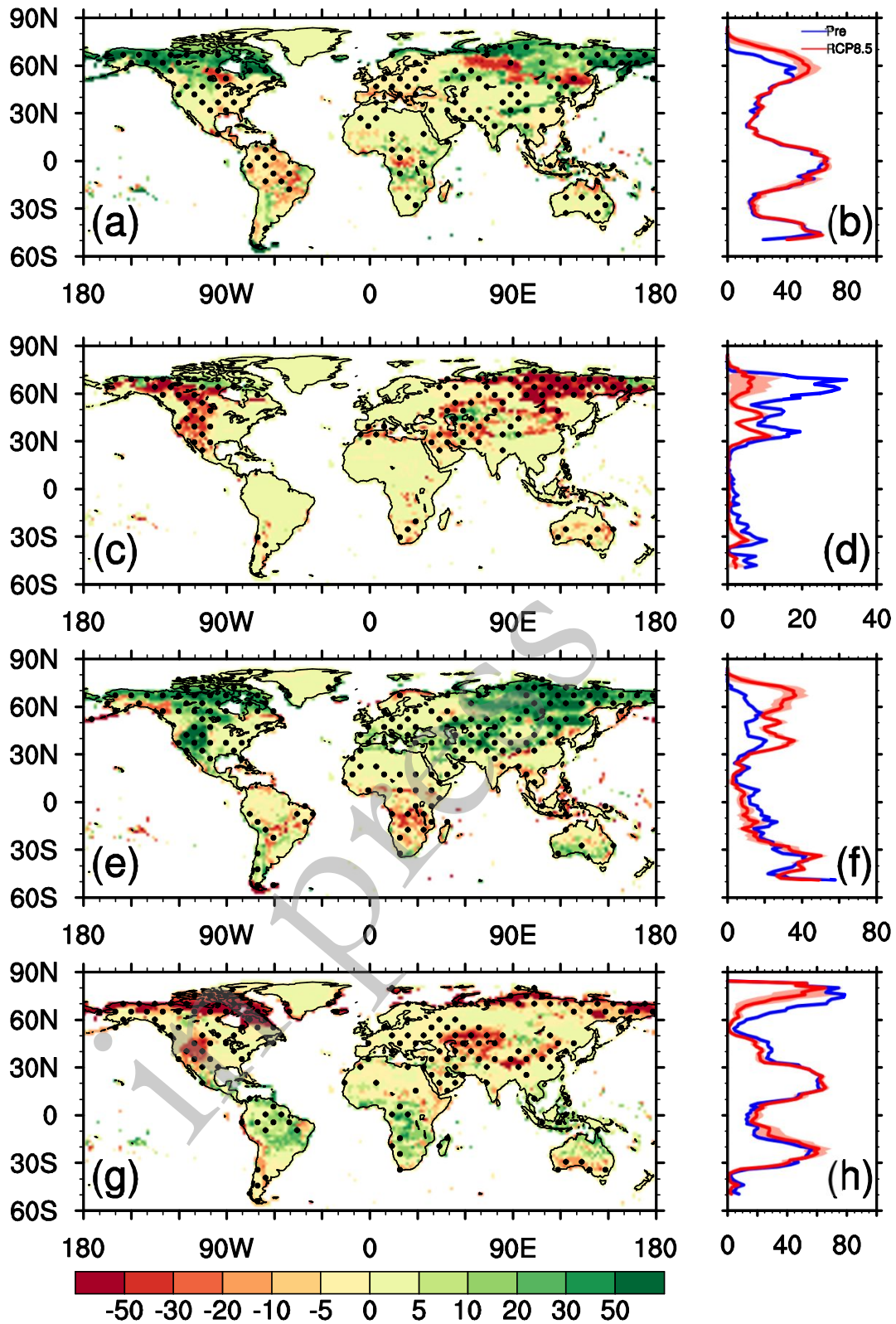
781

782 **Fig. 1.** Projected future changes of (a) annual surface air temperature (K) and (b)

783 precipitation (mm day⁻¹) based on the 16 CMIP5 models. The stippled regions

784 represent grids where at least 14 of 16 models agree with the multi-model ensemble

785 mean.



786

787 **Fig. 2.** Differences in fractional coverage (units: %) of (a) trees, (c) shrubs, (e) grasses

788 and (g) bare ground between the present-day experiment (Pre) and the RCP8.5

789 experiments (RCP8.5) (RCP8.5 minus Pre). The stippled regions represent grids

790 where at least 14 of 16 models agree with the multi-model ensemble mean. (b), (d), (f)
 791 and (h) are the zonal average fractional coverage (units: %) of trees, shrubs, grasses
 792 and bare ground in Pre (blue) and RCP8.5 (red). The shaded red areas represent one
 793 standard deviation.

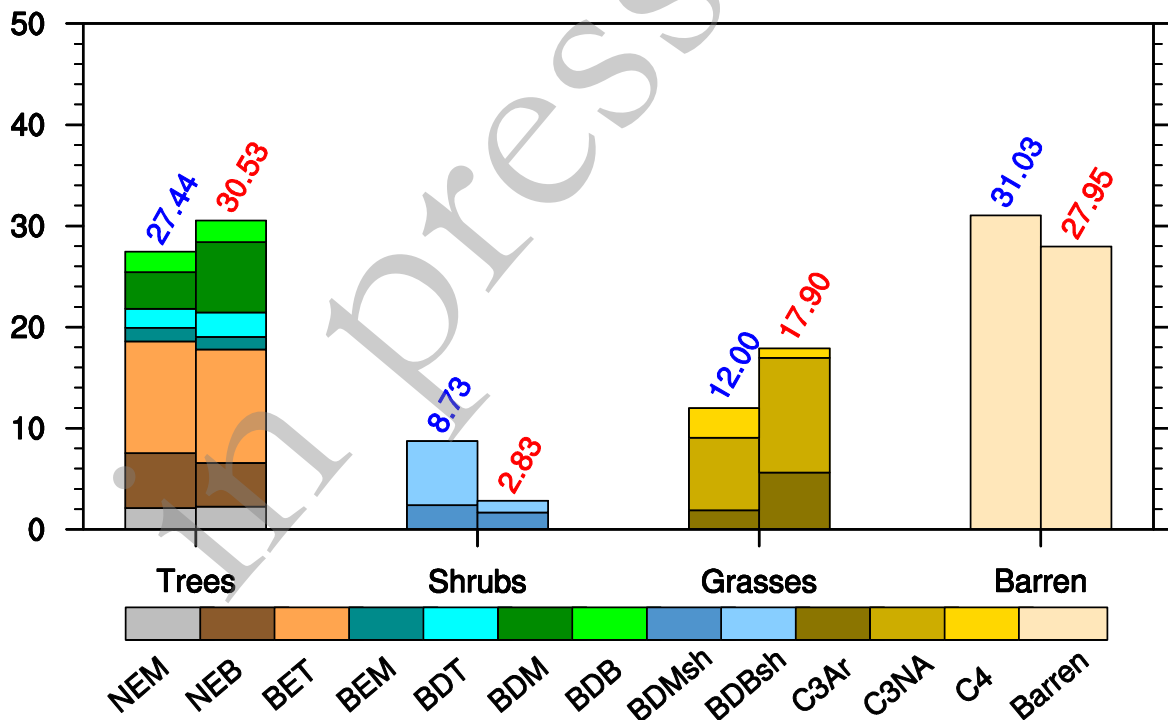
794

795

796

797

798



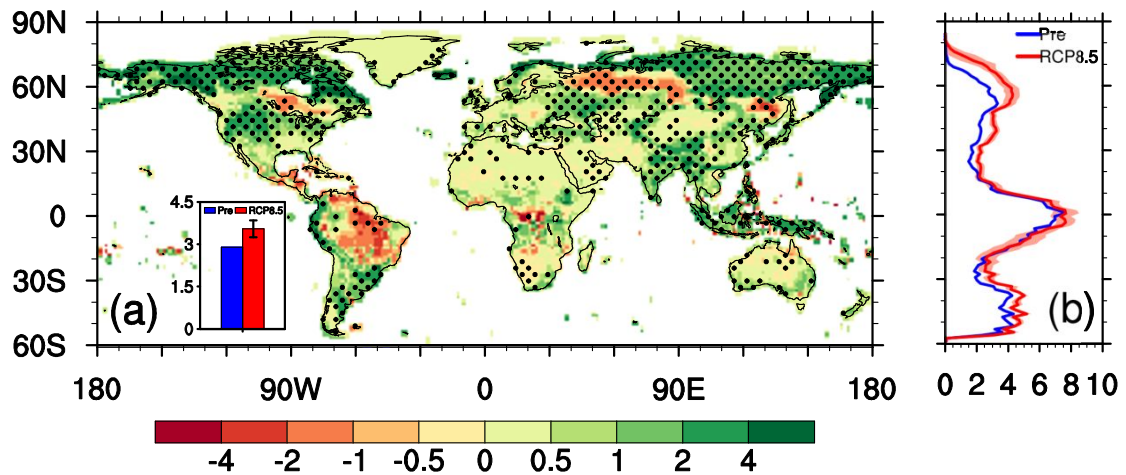
799

800 **Fig. 3.** Global weighted average fractional coverage (%) of each PFT for Pre (blue)

801 and RCP8.5 (red). The abbreviations of the PFT correspond to the information in

802 Table S1.

803



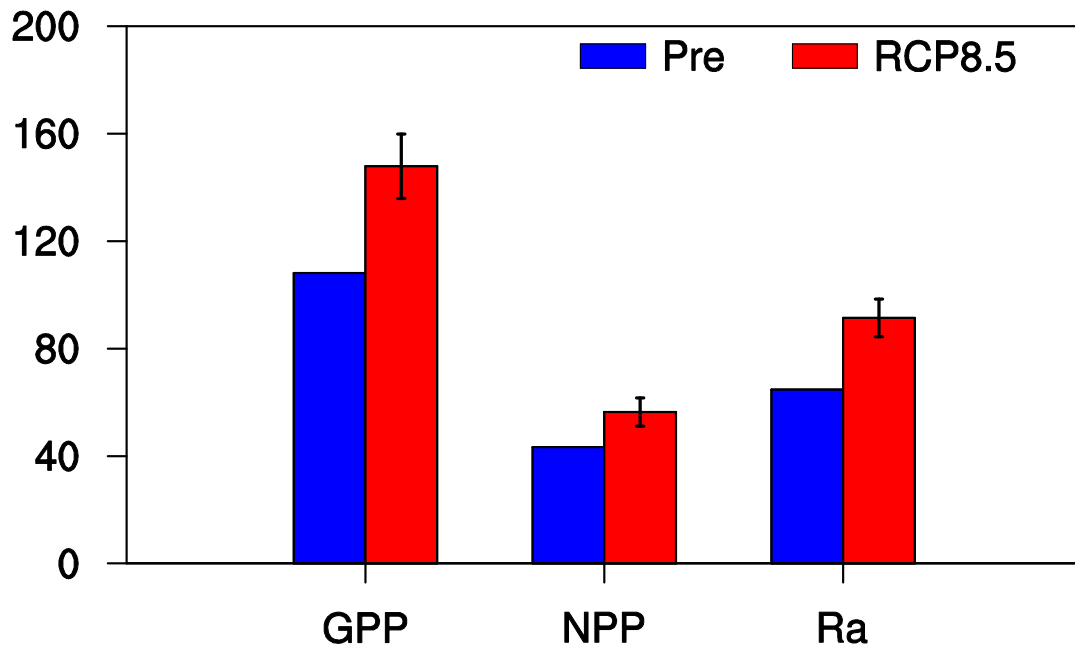
804

805 **Fig. 4.** (a) Spatial distribution of differences in leaf area index (LAI) between Pre and
 806 RCP8.5 (RCP8.5 minus Pre). The stippled regions represent grids where at least 14 of
 807 16 models agree with the multi-model ensemble mean and the bars in the left bottom
 808 represent the global means of LAI in Pre (blue) and RCP8.5 (red). (b) The zonal
 809 average of LAI in the present-day experiment (Pre; blue) and the RCP8.5 experiments
 810 (RCP8.5; red), respectively. The shaded red areas represent one standard deviation.

811 All units are $\text{m}^2 \text{m}^{-2}$.

812

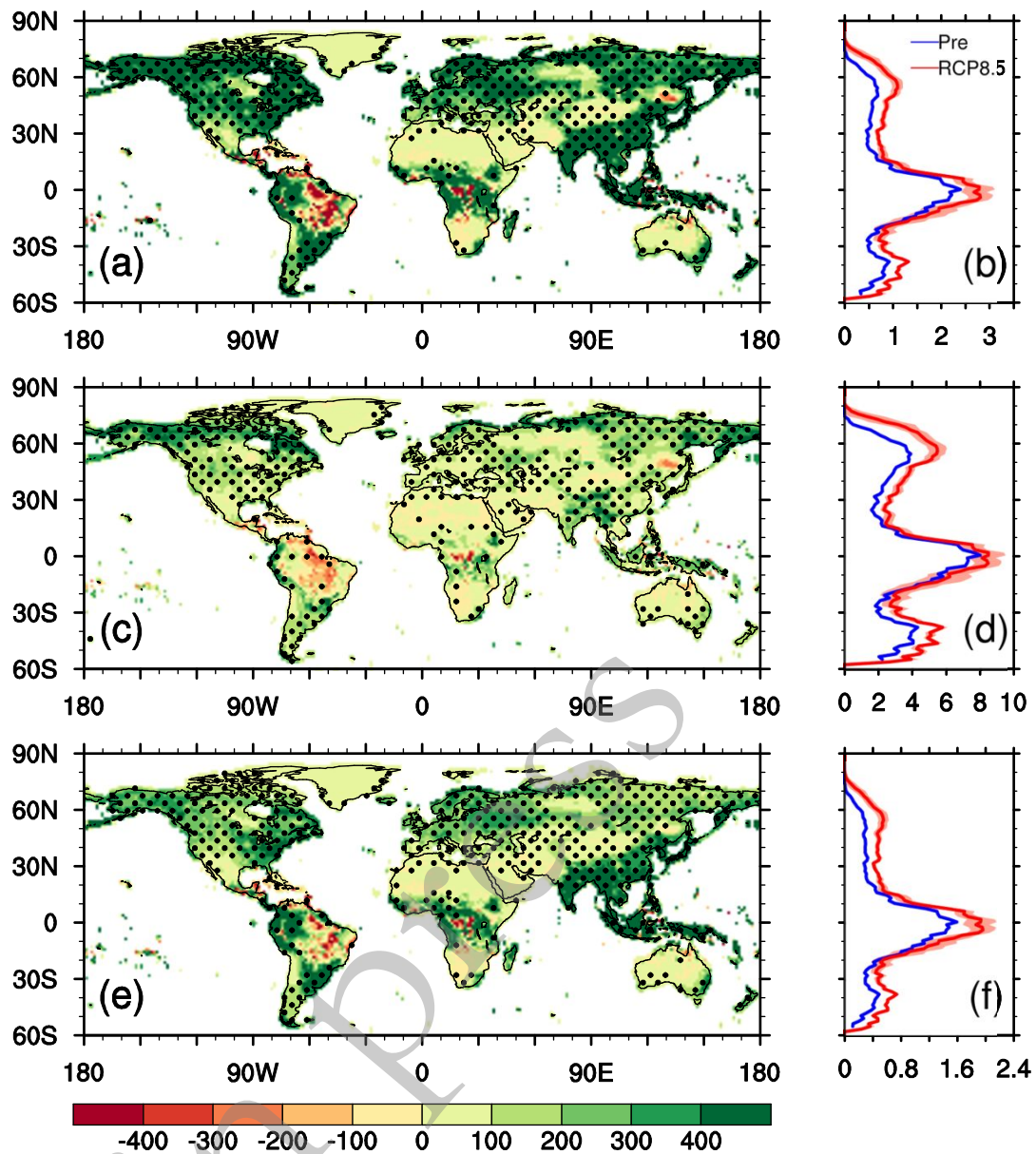
813



814

815 **Fig. 5.** Global means of carbon fluxes in Pre (blue) and RCP8.5 (red). The bars
816 represent one standard deviation. All units are PgC yr⁻¹.

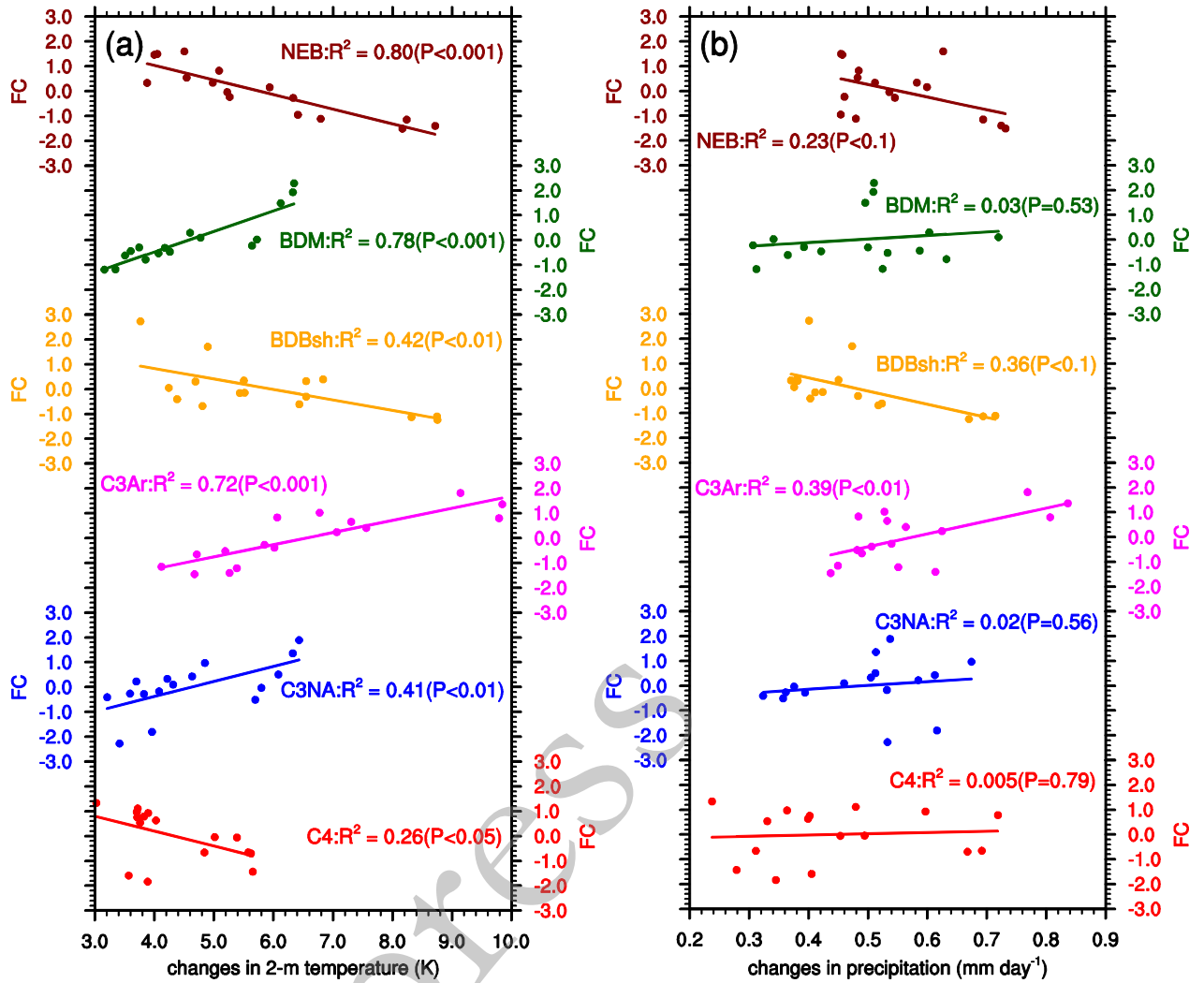
in press



817

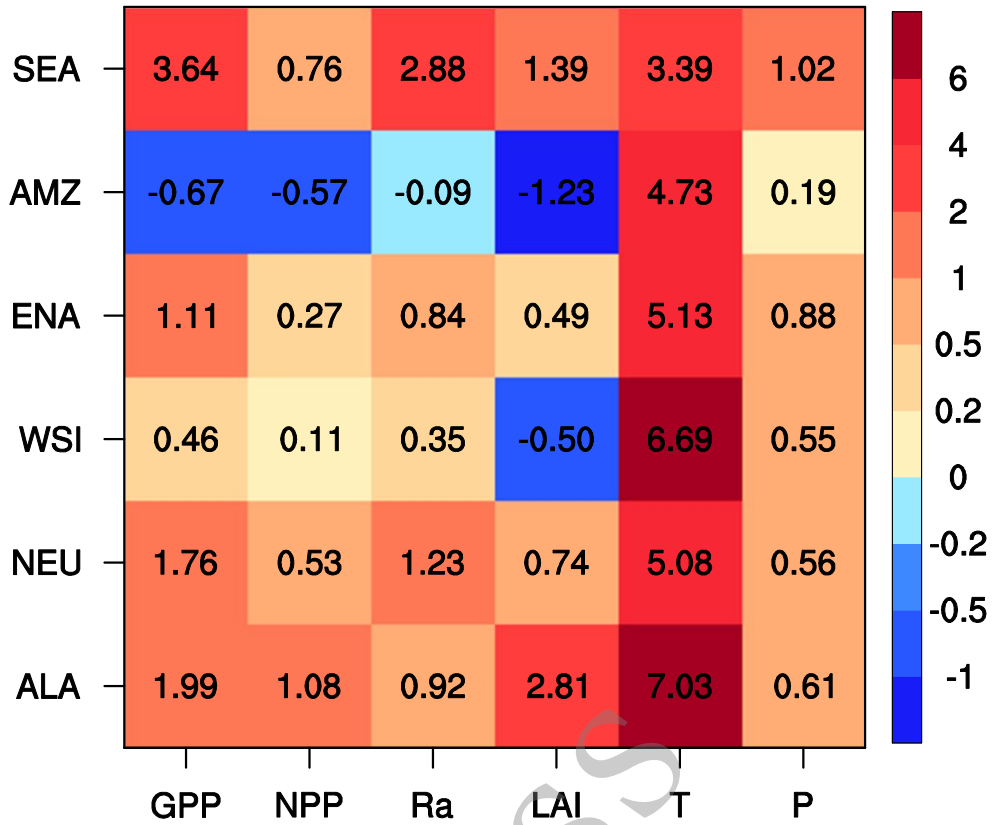
818 **Fig. 6.** Spatial distribution of differences between the present-day experiment (Pre)
 819 and the RCP8.5 experiments (RCP8.5) (RCP8.5 minus Pre) in (a) GPP, (c) NPP and
 820 (e) Ra. (units: $\text{gC m}^{-2} \text{yr}^{-1}$). The stippled regions represent grids where at least 14 of
 821 16 models agree with the multi-model ensemble mean. (b), (d) and (f) are the zonal
 822 average (units: $\text{KgC m}^{-2} \text{yr}^{-1}$) of GPP, NPP and Ra in Pre (blue) and RCP8.5 (red).
 823 The shaded red areas represent one standard deviation.

824



825

826 **Fig. 7.** Relationship between the changes in fractional coverage (FC, %) of the six
 827 PFTs (NEB, BDM, BDBsh, C3Ar, C3NA, C4) with (a) annual mean surface 2-m
 828 temperature (K), and (b) precipitation (mm day⁻¹) among the 16 ensembles. The
 829 changes in fractional coverage have been standardized. The lines represent the
 830 corresponding regression lines. The abbreviations of the PFT correspond to the
 831 information in Table S1.



832

833 **Fig. 8.** Changes in carbon fluxes (GPP, NPP, and Ra; PgC year⁻¹), LAI (m² m⁻²),

834 temperature (T; K) and precipitation (P; mm day⁻¹) over the six selected regions. The

835 abbreviations of these regions correspond to the information in Table S4.